RSC Advances

Investigation of the Modified Sodium Alginate-Alkyl Glycoside Interactions in Aqueous Solutions and at the Oil - Water Interface

Journal:	*RSC Advances*
Manuscript ID	RA-ART-02-2016-003650.R1
Article Type:	Paper
Date Submitted by the Author:	04-Apr-2016
Complete List of Authors:	Huang, Junhao; Hainan University, College of Materials and Chemical Engineering Li, Jiacheng; Hainan University, College of Materials and Chemical Engineering Feng, Yuhong; Hainan University, College of Materials and Chemical Engineering Xiang, Fei; Hainan University Wang, Rui; Hainan University Wu, Jianbo; Hainan University Yan, Huiqiong; Hainan University Chen, Kai; Hainan University Zhou, Qingfeng; Hainan University Liu, Yanfeng; Hainan University
Subject area & keyword:	Soft matter < Physical

RSC Advances

ARTICLE

Investigation of the Modified Sodium Alginate-Alkyl Glycoside Interactions in Aqueous Solutions and at the Oil -Water Interface

Received 00th January 20xx,
Accepted 00th January 20xx

DOI: 10.1039/x0xx00000x

www.rsc.org/

Junhao Huang [a], Jiacheng Li [a,*], Yuhong Feng [a], Fei Xiang [a], Rui Wang [a], Jianbo Wu [a], HuiQiong Yan [b] Kai Chen [a], Qingfeng Zhou[a] and Yanfeng Liu[a]

Abstract: The interaction of cholesteryl-grafted sodium alginate derivative (CSAD) and decyl-β-D-glucopyranoside (DGP) in solutions was studied through surface tension method, fluorescence spectroscopy, electron paramagnetic resonance (EPR), and dynamic light scattering. Results showed that DGP and CSAD exhibit competitive adsorption behaviour at the water–gas interface and that this competitive behaviour can be intensified by NaCl. EPR revealed that the cholesterol groups of CSAD participate in the formation of micellar structures. The steric effect of cholesterol groups reduces the microviscosity of the micellar structure, but high-concentration NaCl can weaken the polarity and increase the microviscosity of the formed micellar structure. In addition, at a high DGP concentration, high-concentration NaCl can facilitate DGP precipitation; this condition causes abnormal phenomena of surface tension, fluorescence spectroscopy, and EPR. For the emulsion system, analysis of particle size and rheology indicated that DGP and CSAD form a network structure between oil and water interfaces through interaction and thus enhance the non-Newtonian fluid property of the emulsion. Owing to the competitive adsorption between CSAD and DGP at the oil–water interface, DGP gradually replaces CSAD with the increase in DGP concentration. With a further increase in DGP concentration, the stable steric effect of polymers between oil drops may disappear, and oil drops may aggregate mutually.

1. Introduction

Owing to the association between polymers and surfactants, a complex system performs better than a single surfactant or polymer system in terms of higher surface activity of the compound system as well as enhanced decontamination, emulsification, and bubbling behaviour of the surfactant [1]. Therefore, the polymer–surfactant compound system has been widely applied in numerous fields, including detergents, food, coatings, cosmetics, medicines and oil extraction [2, 3]. Polymer–surfactant interaction in solutions and interfaces has attracted much research interest [4, 5]. On the basis of previous work on polymer–surfactant interaction in solutions, different models of the polymer–surfactant interaction have been proposed. Shirahama et al.[6] studied a polyethylene oxide (PEO)/sodium dodecylsulfate (SDS) system through electrophoresis. They found that SDS attaches onto a hydrophobic polymer chain as an analogous micellar structure cluster and that the SDS micellar structure appears to be similar to “pearls on a necklace”. On this basis, the group proposed the “pearl necklace” model. Nagrajan [7] proposed a “sphere” model to describe the ion-dipole effect between the dipole of hydrophilic groups on polymer chains and the head groups of surfactant ions. Owing to the interaction between the polymer hydrophobic chain section and exposure section of the hydrocarbon region of the surfactant micellar structure, the entire system appears as a sphere. This condition narrows the exposed surfactant hydrophobic area and shields electrostatic repulsion between head group charges. Chari et al. [8] analyzed the influence of SDS on local chain movement and long-range size of PEO coil through small-angle neutron scattering, viscosity, and ^{13}C nuclear magnetic resonance (NMR). The team reported that compared with free coils in a good solvent, PEO coils that achieve saturated association with the SDS micellar structure are more intumescent. However, these coils do not expand fully and appear like “intumescent cages”. These models generally have the same basic opinion on hydrophobic-driven association but show a certain difference in microstructure expressions. This variation may be caused by different observation scales of the polymer–surfactant interaction. Our previous model based on research on the interaction between cholesteryl-grafted sodium alginate derivative (CSAD) and N-octyl-β-D-glucopyranoside (OGP) [9] was also established on the basis of these models.

[a] *College of Materials and Chemical Engineering, Hainan University, Hainan, Haikou* 570228*, P. R. China.*
[b] *College of Chemistry and Chemical Engineering, Hainan Normal University, Hainan, Haikou* 571158*, P. R. China.*
† Electronic Supplementary Information (ESI) available: See
DOI: 10.1039/x0xx00000x

Understanding the interaction of polymer–surfactant systems at fluid interfaces (water/air or water/oil) is essential for their proper use in applications, such as in detergency or stabilization of dispersed systems (emulsions, foams, or thin films), in food, pharmaceutical, and cosmetic industries, and in controlled drug delivery and oil recovery [4]. Casford et al. [10] studied the coadsorption of SDS and PEO at the hydrophobic octadecane thiol/aqueous solution interface through sum frequency spectroscopy. The team found that as the surfactant concentration increases, SDS is adsorbed from mixed solution of the polymer, and the surfactant progressively displaces the previously adsorbed PEO. Petrovic et al. [11] investigated the interaction between hydroxypropylmethyl cellulose (HPMC) and sodium dodecylsulfate and its influence on oil/water (o/w) emulsion properties. The HPMC/SDS complexes, which are formed in the interaction region, enhance the continuous phase and emulsion viscosity. The network formed by HPMC–SDS intermolecular binding contributes to a more compact structure of the emulsion adsorption layer. Marshall et al. [12] studied the small-angle neutron scattering of gelatin / SDS complexes at the polystyrene–water interface. The adsorbed layer thickness as a function of contrast-matched SDS concentration/adsorption increases to the maximum value at approximately the saturation point, and the volume fraction of the polymer adsorbed at the interface diminishes simultaneously. Akiyama et al. [13] emphasized the emulsification mechanism by using hydrophobically–hydrophilically modified hydroxyethylcellulose (HHM–HEC) and a lipophilic surfactant. The 3D network structure of HHM–HEC can hold oil particles, including the lipophilic surfactant, without the occurrence of phase inversion. Philip et al. [14, 15] investigated the interaction of poly(vinyl alcohol) and a surfactant at the liquid droplet interface. The addition of a surfactant causes conformational changes in the polymer coil and leads to "stretched tail-like" conformation because of bound surfactant molecules. As the surfactant concentration increases, an increasing amount of surfactant molecules and micelles enter the folded chains, stretching the loops further. Overall, competitive adsorption occurs between the polymer and surfactant at fluid interfaces. For the emulsion system, the polymers and surfactants can interact and form a 3D network structure to increase the distance between oil particles and the viscosity of the systems; this condition contributes to the stability of the emulsion system.

Sodium alginate is a natural anionic polyelectrolyte that possesses good biocompatibility and biodegradability. It has been extensively utilized in pharmaceutical preparation, cosmetics, tissue engineering, food, and other fields because of its unique physicochemical properties. However, the strong hydrophilicity of the material limits its practical industrial applications to a certain extent. Modification [16] can bestow new characteristics to sodium alginate without affecting the original biological characteristics. Alkyl polyglycoside (APG), an internationally accepted first-choice "green" functional surfactant, inherently has good biodegradability, is environmentally friendly, and has low dermal toxicity [17]. We have studied the stable emulsion of CSAD and industrial APG [18] and found that the emulsion system is relatively stable when the CSAD concentration is 1 $g \cdot L^{-1}$. However, we did not explore the related microscopic mechanism. In the current study, the influence of NaCl on CSAD–decyl-β-D-glucopyranoside (DGP) interaction and the behaviour at the liquid–drop interface were discussed (see Fig. 1 for the structure). Moreover, competitive adsorption behaviour at the gas–liquid interface, aggregation behaviour in water solutions of CSAD and DGP, and the influence of NaCl on the interaction were analyzed through surface tension method, fluorescent spectrometry, and EPR. Emulsions of corresponding mixing ratios were prepared to test particle size distribution and rheological property. We also illustrated the possible interaction mechanism between CSAD and DGP at the oil–water interface. The conclusion is that high-concentration NaCl can significantly influence CSAD–DGP interaction but presents disadvantages for emulsion stabilization. At the oil–water interface, CSAD and DGP can stabilize emulsion by forming a network structure. High-concentration DGP impedes emulsion stability because of the competitive adsorption behaviour of CSAD and DGP at the oil–water interface.

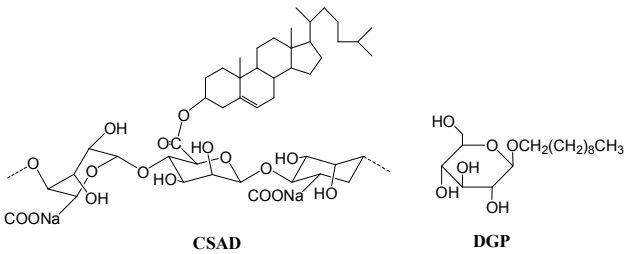

Fig. 1. Structures of CSAD and DGP

2. Materials and methods

2.1. Materials

Alginic acid (CP degree, M_W=7.3 × 10^5), cholesterol (AR degree, M_W= 386.6), calcium hydride (AR degree), N,N'-dicyclohexylcarbodiimide (DCC, 90.0%), 4-(N,N'-dimethylamino) pyridine (DMAP, 99%), dimethyl sulfoxide (DMSO, AR degree), chloroform (AR degree), and Decyl-β-D-Glucopyranoside (BC degree) were purchased from the Aladdin Company. Absolute ethyl alcohol (AR degree), xylene (AR degree), sodium chloride (AR degree) and sodium bicarbonate (AR degree) were from Guangzhou Chemical Regent Factory, whereas 5-doxyl stearic acid and pyrene (GC, ≥99.0%) was purchased from Sigma Company. The water is the redistilled water (18.2 mΩ·cm).

2.2 Synthesis of CSAD

Detailed procedure of the synthesis is described in our previous paper[9]. Briefly, alginic acid (1.0 g, 5.68 mmol hexuronic acid residues) was added to dimethyl sulfoxide (30 ml) that was dried for five days by calcium hydride. The mixture was gently stirred into a suspension at 50 °C overnight. After addition of DCC (0.416 g, 2.02 mmol), DMAP (0.492 g, 4.03 mmol) and a solution of chloroform (3 mL) containing cholesterol (0.65g, 1.68 mmol) were also added. The reaction between the carboxylic acid groups of alginic acid and the hydroxyl of cholesterol was allowed to proceed at 40 °C for 24 h. The product was precipitated completely from the above mixture by adding ethanol, filtrated, and then washed successively with ethanol. The solid product obtained was dissolved in distilled water and neutralized by adding 4% $NaHCO_3$ solution. The solution was dialyzed against water for four days to remove the low-molecular weight impurities and then lyophilized to obtain pure CSAD product. The FTIR spectra and H^1-NMR spectra of CSAD are seen in Supplementary Information (see Fig. S1 and Fig. S2 of Supplementary Information). The molecular weight (M_W) of CSAD is 1.1×10^5 (see Fig. S3 of Supplementary Information)

2.3. Preparation of emulsions

Continuous phases of the emulsions were prepared by mixing required amounts of CSAD and DGP stock solutions to obtain a total CSAD concentration of 1 g·L^{-1} and the desired DGP concentration in the range of 0.00 mmol·L^{-1} to 4.00 mmol·L^{-1}. Emulsions were prepared by dispersing 8% v/v xylene in the continuous phase by means of a SCIENTZ-11E ultrasonic homogenizer (Ningbo, China) for 10 min with 4 s intervals after each 3 s of ultrasonication at 700 W. The mixtures were placed in a cold water bath to avoid overheating of the samples. To reassure about the influence of ultrasonication, the molecular weight (M_W) of CSAD was measured by gel permeation chromatography (GPC) which is conducted by a Waters 2695 (USA) high performance liquid chromatography before and after ultrasound pretreatment. The structure of CSAD was not broken by ultrasonication since the molecular weight of CSAD did not have a decrease (see Fig. S3 of Supplementary Information).

2.4. Surface tension measurement

Solutions were prepared in different concentration ratios. Equilibrium surface tension was measured under 25 °C with plate method by JK99C automatic tension meter (Shanghai, China); the final data should be the average value of three measurements.

2.5. Fluorescence spectrum measurement

Probe (pyrene) concentration was maintained at a constant concentration of 1×10^{-6} mol·L^{-1}. Steady-state fluorescence experiments were performed with F7000 molecular fluorescence spectrometer (Hitachi, Japan). The measurement conditions were as follows: wavelength, 335 nm and spurred by fluorescence spectrum; wavelength scanning scope, 335–600 nm; widths of slits, 2.5 nm; and excitation voltage, 700 V.

2.6. Size analysis

The size distributions of the solutions and emulsions were determined with a Zetasizer Nano ZS90 (Malvern, UK), which is a highly sensitive dynamic light scattering instrument. The analyzer adopts a He–Ne light source with 10 mW power, 633 nm wavelength, measuring angle of scattering intensity of 90°, and measuring temperature of 25 °C. Emulsion droplets were obtained after appropriate dilution of the sample with water. We confirmed in advance that the dilution process does not significantly change the particle size. In addition, a minimum of three separately prepared replicates were measured for all samples.

2.7. Electron paramagnetic resonance (EPR)

The EPR spectra were recorded at 9.56 GHz with a Bruker EPR spectrometer A320 (Bruker, Germany). All measurements were conducted at room temperature by using a quartz tube with an external diameter of ~1.5 mm. Spectra were recorded at an 80 G scan range, 100 kHz magnetic field modulation, and 1 G modulation amplitude. The spin probe concentration was maintained at a constant concentration of 5×10^{-5} mol·L^{-1}, which is usually regarded as negligible perturbation to the micelle structure. The samples were stirred for 1 h and then stabilized for 2 h at room temperature prior to measurements.

2.8. Rheological measurements

The rheological properties of all the emulsions were measured with a DHR-2 (TA Instruments) rheometer equipped with a parallel plate geometry (60 mm diameter and 500 μm gap). The experiments were performed in the flow ramp test, which was established for each sample at a shear rate of 0.01 and 1000 s^{-1}. The equilibration time is 5.0 s and the averaging time is 30.0 s. The rheometer was equipped with a Peltier control system that allows the accurate control of temperature (25 ± 0.1 °C).

3. Results and discussion

3.1. Interaction of CSAD and DGP in aqueous solutions

3.1.1. Surface Tension

The variation in surface tension with the concentration of the DGP surfactant is shown in Fig. 2. Curves a and b show that the surface tension of the solutions increase slightly and reach a plateau when the DGP concentration is low. Surface tension considerably decreases with the increase in DGP concentration.

CSAD is adsorbed at the gas–liquid interface, resulting in competitive adsorption with DGP. In the presence of 0.1 mol·L^{-1} NaCl, the surface tension of the solutions decreases considerably when the DGP concentration is low. CSAD stretches more at the gas–liquid interface because of the shielding effect of NaCl. In addition, CSAD becomes more coiled in the bulk and is unlikely to adsorb with DGP because of the high NaCl concentration. Yang [19] studied the self-assembly behaviour of amphiphilic CSAD in an aqueous solution and reported that the presence of NaCl benefits the self-assembly behaviour of CSAD. The critical micelle concentration (CMC) of DGP is 2.7 mmol·L^{-1} in aqueous solutions. The CMC of the solution with 1 g·L^{-1} CSAD decreases to 2.15 mmol·L^{-1}, whereas that of the solution with 0.1 mol·L^{-1} NaCl and 1 g·L^{-1} CSAD is 2.42 mmol·L^{-1}. When the DGP concentration is higher than CMC, the surface tension curve shows an abnormal increase because of the presence of 0.1 mol·L^{-1} NaCl. The high NaCl concentration benefits DGP micellization, and DGP separates from the solution. During the experiment, a certain amount of DGP precipitation was visible on the bottom of the tube. Lima et al. [20] also have found salt-induced phase separation. Though the aggregation number of decyltrimethylammonium triflate micelles has a limited increase at high sodium triflate concentration, the interaggregate repulsion from micelles decreases and leads to phase separation.

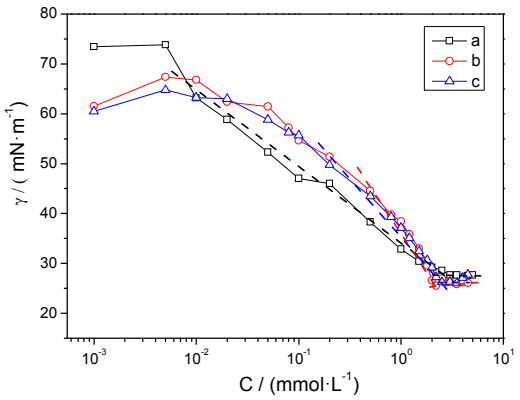

Fig. 2. Surface tension as a function of the DGP solutions at 298K (a) DGP, (b) 1 g·L^{-1} CSAD + DGP, (c) 1 g·L^{-1} CSAD + 0.1 mol·L^{-1} NaCl + DGP

3.1.2. Fluorescence study

The variation in the I_1/I_3 and I_e/I_m values of pyrene as a function of DGP concentration is shown in Fig. 3. The plots present the usual sigmoid shape with a rapid decrease in I_1/I_3 values at DGP concentrations slightly below CMC; stabilization is exhibited at high DGP concentrations. The sharp break in the curve represents the transfer of pyrene from high polarity to low polarity and a more hydrophobic environment, which corresponds to the formation of aggregates [9]. As shown in Fig. 3A, when the DGP concentration is low, the I_1/I_3 values of the solution increase slightly in the presence of 1 g·L^{-1} CSAD. The previous aggregations reassemble into micelles with increased microenvironment polarity because part of DGP is adsorbed with CSAD and affects the interaction of the two compounds. Then, the I_1/I_3 values of the solution decrease gradually with the increase in DGP concentration. When the DGP concentration is higher than the critical aggregation concentration (CAC) of 0.5 mmol·L^{-1}, the I_1/I_3 values dramatically decrease, thereby forming polymer–surfactant complexes because of the interaction between CSAD and DGP. When the concentration of OGP reaches approximately 3 mmol·L^{-1}, which is the adsorbed saturation concentration (C_2), the adsorption amount of OGP on the CSAD molecular chain reaches saturation, the DGP monomer micelle structures begin to form in the solution, and the microenvironment of micelles becomes stable. These results indicate that I_1/I_3 values remain stable at a certain constant. The CMC of the solution with 1 g·L^{-1} CSAD is 1.8 mmol·L^{-1}, that of the solution with 0.1 mol·L^{-1} NaCl and 1 g·L^{-1} CSAD is 1.67 mmol·L^{-1}, and that of the DGP solution is 2.03 mmol·L^{-1}. For the solution system with 0.1 mol·L^{-1} NaCl and 1 g·L^{-1} CSAD, considerably smaller I_1/I_3 values are produced compared with the solution with 0.1 g·L^{-1} CSAD when the concentration of DGP is below CAC. This finding indicates that CSAD forms more compact micelles by self-assembly because of the presence of 0.1 mol·L^{-1} NaCl. The molecular mechanic simulations from Ribeiro group[21, 22] can help us to find the reasons. Sodium cations crucially effect the conformation of sodium alginate, and the alginic acid coordinates and folds around cation quite easily. Owing to the effect of NaCl, the micellar environment cannot remain stable, and the I_1/I_3 values vary at approximately 1.45 at a low DGP concentration. A plateau exists until the DGP concentration exceeds 0.1 mmol·L^{-1}. With the increase in DGP concentration, the I_1/I_3 values of the solution rapidly decrease. In addition, the I_1/I_3 values exhibit a similar abnormal increase as the surface tension curve when the DGP concentration exceeds 3.5 mmol·L^{-1}, proving that high NaCl concentration benefits micellization and precipitation of DGP.

The change in I_e/I_m values is usually employed to study the change in the number of hydrophobic micro areas in the solution. The change also reflects the variation in micellar polarity. In Fig. 3B, the I_e/I_m values reach the peak and rapidly decrease with the increase in DGP concentration when the DGP concentration reaches approximately 2 mmol·L^{-1}. This result indicates that the number of molecules drastically increases and the CMC of DGP is close. For the solution with 1 g·L^{-1} CSAD, the peak is not sharp, unlike that of the DGP solution, and the I_e/I_m value is smaller because single DGP molecular micelles cannot rapidly form owing to the formation of CSAD and DGP complexes. For the solution with 0.1 mol·L^{-1} NaCl and 1 g·L^{-1} CSAD, the I_e/I_m values fluctuate within a low DGP

concentration range because of high NaCl concentration. At a high DGP concentration, the I_e/I_m values also exhibit an unexpected increase, which is in agreement with the I_1/I_3 and surface tension curve.

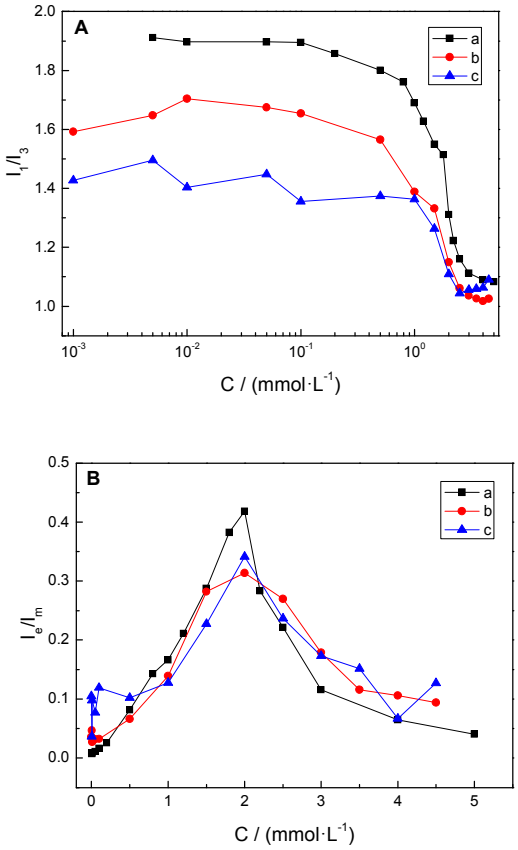

Fig. 3 Variation of I_1/I_3 and I_e/I_m values of pyrene as a function of the DGP concentration: (a) DGP, (b) 1 g·L^{-1} CSAD + DGP, (c) 1 g·L^{-1} CSAD + 0.1 mol·L^{-1} NaCl + DGP

3.1.3. Dynamic light scattering (DLS)

The hydrodynamic diameter distribution of the mixed solution with 1 g·L^{-1} CSAD is shown in Fig. 4A. The CSAD–DGP interaction is similar to the CSAD–OGP interaction [9]. At a low DGP concentration, the DGP molecules facilitate interactions between CSAD molecules. The CSAD molecules form a denser micellar structure, and the hydrodynamic diameter decreases. As the DGP concentration increases, the DGP molecules are adsorbed onto CSAD and form polymer–surfactant complexes. The polymer–surfactant complexes achieve the largest hydrodynamics diameter when the DGP concentration is approximately equal to CMC. With the further increase in DGP concentration, the formed polymer–surfactant complexes are damaged by high-concentration DGP and form "pearl necklace" surfactant–polymer complexes decorated by the DGP micellar structure. The hydrodynamics diameter of the "pearls" on the pearl necklace structure complexes is significantly smaller than that of the polymer–surfactant complexes. DGP adsorption onto CSAD reaches saturation at approximately 3 mmol·L^{-1}, and more pearl necklace structure complexes are present in the solution. With the continuous increase in DGP concentration, the pearl necklace structure complexes interact with one another and develop "core-shell" surfactant–polymer complexes with an increased hydrodynamic diameter. The microenvironments of the pearl necklace structure complexes and core-shell structure complexes tend to be stable, and the I_1/I_3 value of the solution changes slightly. As the DGP concentration continues to increase, the DGP monomer micellar structure begins to appear and develop in the solution. The micellar structure of the DGP monomer possesses a small hydrodynamic diameter and averages the hydrodynamic diameter of the solution.

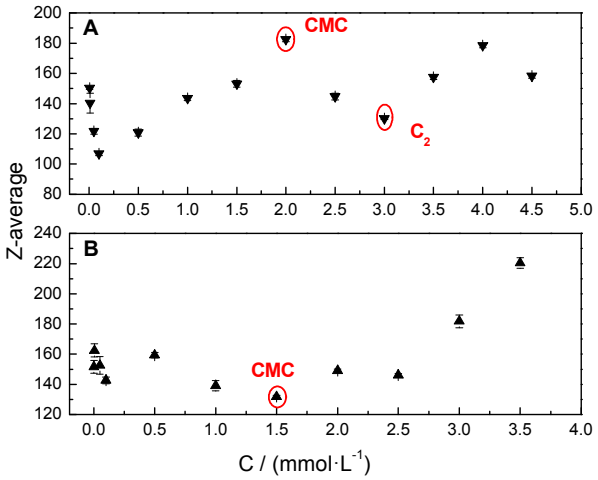

Fig. 4. Hydrodynamic diameter of aqueous [poly(CSAD/DGP)] solution without (A) and with (B) 0.1 mol·L^{-1} NaCl as a function of the DGP concentration

The hydrodynamic diameter distribution of the mixed solution with 0.1 mol·L^{-1} NaCl and 1 g·L^{-1} CSAD is shown in Fig. 4B. Compared with that of the solution without NaCl, the hydrodynamic diameter of this mixed solution fluctuates gradually around 160 nm at a low DGP concentration. This finding is in agreement with the fluorescence spectrum and presents the collaborative consequence of reinforcing and shielding effects of NaCl that deteriorate micellar structure stability. When the DGP concentration is less than 0.5 mmol·L^{-1}, CSAD mainly forms analogous micellar structures through molecular interaction at high NaCl concentrations. As the DGP concentration increases, the analogous micellar structures decompose and form pearl necklace structure complexes directly. Owing to the reinforcing effects of high-concentration NaCl, DGP reaches CMC at approximately 1.5 mmol·L^{-1}. At this point, the

hydrodynamic diameter of the solution is close to that of the mixed solution without NaCl at C_2. With the further increase in DGP concentration, pearl necklace structure complexes interact with one another and develop core-shell structure complexes, thereby increasing the hydrodynamic diameter of the solution.

3.1.4 EPR

The EPR of 5-free radical nitroxide–stearic acid in different environments is shown in Fig. 5. Curve a shows the EPR spectrum when C_{DGP} = 1.2 mmol·L^{-1} (lower than CMC of DGP). The probe is in a uniform polarity environment, and three peaks of the EPR spectrum (low field, central field, and high field peaks) are basically of the same height. With the increase in DGP concentration (<CMC), all three peaks (curve b) begin to show some deformation. When the DGP concentration exceeds CMC, the heights of the three EPR peaks (curve c) become different, accompanied by an increasing peak width. This finding is due to the condition that probe molecules are in two environments with different polarities: solvent continuous phase with strong polarity and micellar structures or aggregate surface with weak polarity. The spectrum generated in different environments possesses different g values. The superposition of the peaks of two different g values will change both peak height and width [23]. Given that the probe molecules are in two different environments, the three EPR peaks on curve d and e present different peak heights and increased peak widths. However, the peak–peak width is narrower than that of same-concentration DGP solution, indicating that the microenvironment of the formed micellar structure is weaker.

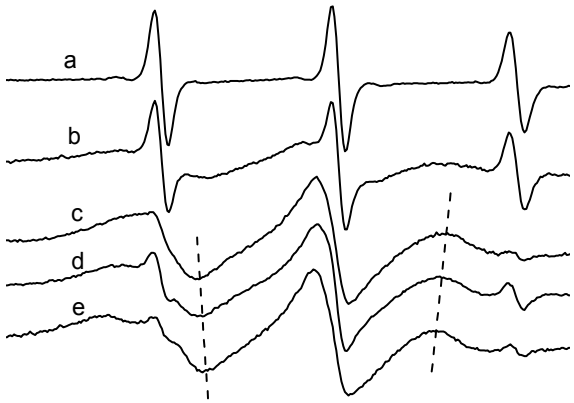

Fig. 5. The EPR spectrum of 5-doxyl stearic acid in different solution: (a) C_{DGP} =1.2 mmol·L^{-1}; (b) C_{DGP} =2.0 mmol·L^{-1}; (c) C_{DGP} =3.0 mmol·L^{-1}; (d) 1 g·L^{-1} CSAD, C_{DGP} =3.0 mmol·L^{-1}; (e) 1 g·L^{-1} CSAD + 1 mol·L^{-1} NaCl, C_{DGP} =3.0 mmol·L^{-1}.

The hyperfine coupling constant (A_N) can reflect the polarity of the microenvironment in which the probe molecules are located. High microenvironment polarity results in the electron density of free radical nitroxide. In other words, high A_N implies high microenvironment polarity of the probe [23]. Studies [24, 25] have demonstrated that according to the A_N of EPR, the environment of free radical nitroxide is composed of approximately 55% water and 45% hydrocarbon. Spinning probe molecules are close to the micellar structure surface, indicating that stearic acids are at the micellar structure–water interface and are inserted into the stern layer of the micellar structure [24-26]. Fig. 6 shows the relation curve between A_N of the probe molecular and DGP concentration at room temperature. Curve a shows that the A_N values are about 15.8 G when the DGP concentration is lower than 2.5 mmol·L^{-1} but declines quickly to 11.59 G when the DGP concentration exceeds 2.5 mmol·L^{-1}. With the further increase in DGP concentration, A_N decreases to approximately 11.20 G and reaches a constant value. The sharp reduction in A_N indicates that 5-free radical nitroxide–stearic acid probes transfer from a continuous phase with strong polarity to the surface of micellar structure aggregates with weak polarity. This mechanism is the formation process of micellar structure aggregates. On this basis, CMC of DGP was determined and was found to be about 2.5 mmol·L^{-1}. This finding is in accordance with the surface tension and fluorescence spectrum. For curve b and c, A_N is about 15.8 G when the DGP concentration is less than 2.5 mmol·L^{-1}, indicating that the micellar structure consisting of CSAD aggregation and the complex micellar structure formed by CSAD and a few DGP are not very dense, and all micellar structures present strong surface polarity. When the DGP concentration exceeds 2.5 mmol·L^{-1}, A_N reaches a certain level, and the corresponding CMC is considerably lower than that of the DGP solution. The A_N of the solution with 1 g·L^{-1} CSAD is approximately 10.8 G, which is lower than that of the DGP solution. This result implies that the microenvironment of mixed micellar structures presents weak polarity. The A_N of the solution with 1 g·L^{-1} CSAD and 0.1 mol·L^{-1} NaCl is even smaller (10.6 G), which is related to the high micellar structure density caused by the reinforcing effects of NaCl. The A_N of the mixed solution decreases to a certain extent with the increase of DGP concentration. The late rise of curve c is caused by some DGP precipitation under high-concentration NaCl.

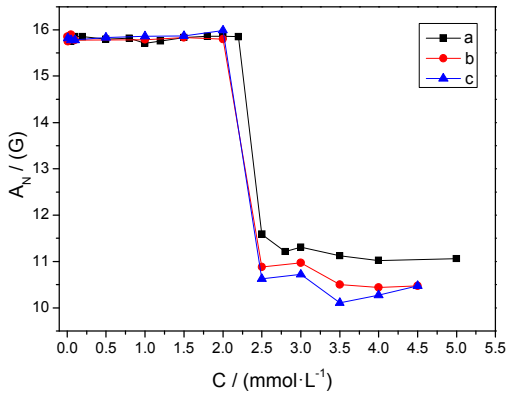

Fig. 6. Variation for A_N of the probe as a function of the DGP concentration at room temperature: (a) DGP, (b) 1 g·L^{-1} CSAD + DGP,
(c) 1 g·L^{-1} CSAD + 0.1 mol·L^{-1} NaCl + DGP

Rotational correlation time refers to the time for free radicals to rotate around the axis for one round. It reflects the viscosity of the microenvironment where probe molecule is located and is particularly applicable to the testing of microviscosity changes in the micellar structure and emulsion surface. τ_c can be calculated from [27]

$$\tau_c = 6.5 \times 10^{-10} \cdot \Delta H_0 [(\frac{h_0}{h_{+1}})^{\frac{1}{2}} + (\frac{h_0}{h_{-1}})^{\frac{1}{2}} - 2],$$

where ΔH_0 is the line width of the EPR central peak and h_{-1}, h_0, and h_{+1} are the heights of low field peak, central field peak, and high field peak, respectively. According to Debye's formula [28], $\tau_c = 2\pi\eta Lr^2/KT$, molecular movement speed τ_c is proportional to microviscosity (η) of the medium environment.

The relation curves between the τ_c of probe molecule solution and DGP concentration at room temperature are shown in Fig. 7. When the DGP concentration is less than 2.0 mmol·L^{-1}, τ_c is small and is basically independent from DGP concentration. At this point, probe molecules rotate quickly, indicating the low viscosity of the microenvironment. With the increase in DGP concentration, the τ_c values of all three curves begin to increase significantly, whereas the rotation of micellar structures or aggregates where probe molecules are located slows down, indicating that the viscosity of microenvironment increases. However, the τ_c of the solution with 1 g·L^{-1} CSAD (curve b) increases more slowly than that of the DGP solution (curve a). This finding may be due to the steric effect of cholesterol groups increasing the particle size of the micellar structure. Therefore, larger motion space is available for probe molecules, and τ_c increases slowly. In the mixed solution with 0.1 mol·L^{-1} NaCl, the reinforcing effect of NaCl makes micellar structure formation easy (resulting in high micellar structure density) and increases the viscosity of the probe microenvironment. When C_{DGP} = 4.5 mmol·L^{-1}, some DGP precipitation decreases the viscosity of the micellar structure microenvironment.

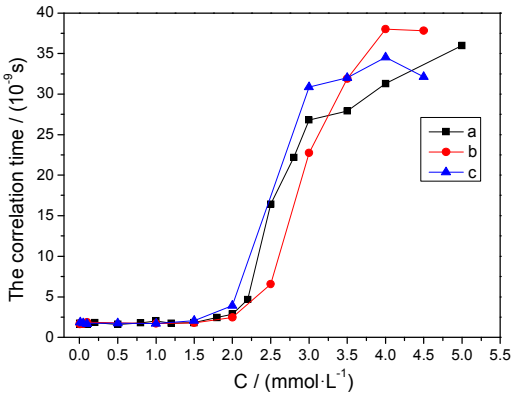

Fig.7. Variation for τ_c of the probe as a function of the DGP concentration at room temperature: (a) DGP, (b) 1 g·L^{-1} CSAD + DGP,
(c) 1 g·L^{-1} CSAD+0.1 mol·L^{-1} NaCl + DGP

3.2. Interaction of CSAD and DGP at the Oil–water Interface

We prepared corresponding emulsions (see Fig. S4 of Supplementary Information) under the same conditions. However, oil–water separation was observed evidently in the emulsion with 0.1 mol·L^{-1} NaCl. High NaCl concentration could weaken emulsion stability because the shielding effect of NaCl reduces electrostatic repulsion between CSAD. Therefore, this paper only discusses the emulsion system without NaCl. The emulsion system without NaCl is unstable when the DGP concentration exceeds 3.5 mmol·L^{-1}.

3.2.1. Droplet-size distribution of emulsion

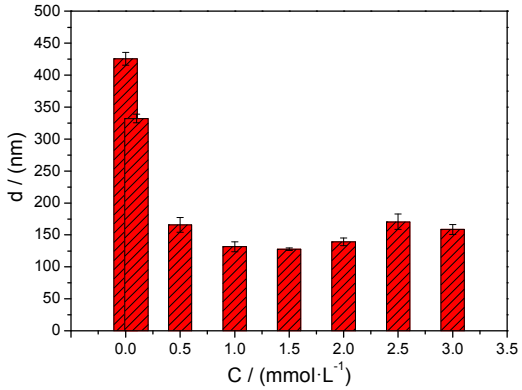

Fig. 8. Mean droplet diameter of CSAD/DGP o/w emulsions prepared from different DGP concentrations on the day of preparation

The oil drop size distribution of emulsions with different DGP concentrations is shown in Fig. 8. The average oil drop size of the emulsion with 1 g·L^{-1} CSAD is 425 nm when C_{DGP} = 0 mmol·L^{-1} and decreases to 332 nm when C_{DGP} = 0.1 mmol·L^{-1}; it is approximately 150 nm when C_{DGP} > CAC. This result is due to the condition that oil drop surfaces are predominantly adsorbed with DGP molecules. When C_{DGP} < CAC, CSAD molecules aggregate on oil drop surfaces mainly through the coil pattern. As DGP concentration increases, DGP molecules occupy the most parts of the oil–water interface, and CSAD molecules extend from the oil–water interface to the continuous phase [15]. When C_{DGP} > 3.5 mmol·L^{-1}, the system cannot form a stable emulsion because high-concentration DGP molecules cause the CSAD molecules to desorb from the oil–water interface. Without steric hindrance of polymers, oil drops easily aggregate, making the emulsion unstable.

3.2.2. Rheological characterization of emulsion

To investigate the CSAD–DGP interaction at the oil drop interface, the steady shear curve of emulsions was tested at 25 °C (Fig. 9A). With the increase in shearing rate, the apparent viscosity of the emulsion decreases continuously until a certain value. Shear thinning of emulsions was observed, indicating that the emulsions belong to pseudoplastic fluids, which are classified as non-Newtonian fluids. The apparent viscosity of the emulsion systems generally increases initially and then decreases as the DGP concentration increases. When C_{DGP} < CAC, the association of several DGP and CSAD molecules enhances the steric hindrance between oil drops, and a large oil drop size increases the apparent viscosity. However, when C_{DGP}>CAC, apparent viscosity decreases because of the small oil drop size.

The power law model [29] was utilized to better describe the rheological properties of the emulsion.

$$\sigma = K\gamma^{m} \ (0 < m < 1), \quad (1)$$

where K is the consistency coefficient and m is the liquidity index. Given that the apparent viscosity is equal to the ratio of shear stress to shearing rate ($\eta_a = \sigma/\gamma$), the apparent viscosity of fluid is described in the power law model as

$$\eta_a = K\gamma^{m-1}. \quad (2)$$

For a pseudoplastic fluid, m < l. In other words, η_a is inversely proportional to γ. Based on the logarithm of Equation (2), we obtain

$$\text{Log } \eta_a = \log K + (m-1) \log \gamma. \quad (3)$$

A straight line can be obtained from the double logarithmic of shear rate and shearing viscosity. m can be calculated from the slope of the straight line, where m = 1 for Newtonian fluids, m < l for pseudoplastic fluids, and m > l for dilatant fluids. The fitting results of the linear region based on the power law model are shown in Fig. 9B. The statistics of m, K and relevant parameters are listed in Table 1. DGP addition reduces m significantly, indicating that the existence of DGP enhances the non-Newtonian property of the emulsion. When C_{DGP} > CAC, m decreases with the increase in DGP concentration, indicating that the non-Newtonian property of the emulsion is enhanced and that the network structure of oil drops is complicated, expanded, and strengthened. However, K remains small during this period because of the small oil drop size. When C_{DGP} > 2.5 mmol·L^{-1}, the m of the emulsion increases rapidly and K decreases, indicating that the network structure of oil drops is damaged by pure DGP micellar structures. This response also explains why high-concentration DGP cannot form a stable emulsion.

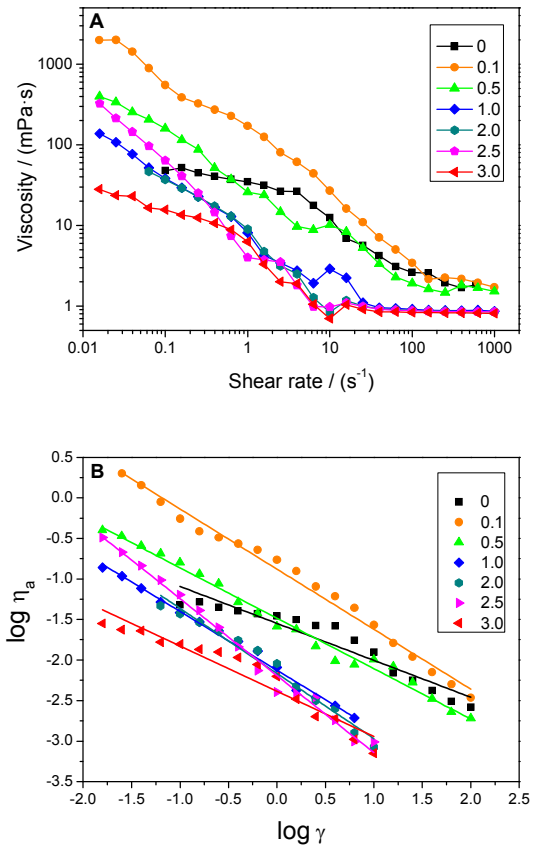

Fig. 9. Rheogram of steady flow measurement (A) and the fitted curve between shear rate and apparent viscosity (B) of emulsion at different DGP concentrations

RSC Advances

ARTICLE

Table 1 The flow index (m), consistency coefficient (K) and relevant parameters of emulsions at different DGP concentrations

C_{DGP} (mmol·L^{-1})	0	0.1	0.5	1	2	2.5	3
Flow Index (m)	0.54	0.26	0.38	0.28	0.2	0.1	0.44
Consistency Coefficient (K)	2.9×10^{-2}	1.3×10^{-1}	3.3×10^{-2}	7.6×10^{-3}	6.9×10^{-3}	7.9×10^{-3}	4.2×10^{-3}
Slope Standard Error	0.0374	0.0187	0.0154	0.0171	0.0376	0.0265	0.0432
Intercept Standard Error	0.0392	0.0209	0.0179	0.0162	0.0263	0.0252	0.0411
R-Square	0.908	0.989	0.988	0.993	0.976	0.989	0.922

3.3 CSAD-DGP interaction mechanisms in aqueous solutions and at the oil-water interface

The mechanism of CSAD–DGP interaction in aqueous solutions and at the oil–water interface is shown in Fig. 10. In Fig. 10a, the CSAD–DGP interaction is similar to the CSAD–OPG interaction [9]. However, given the different side chain lengths of DGP and OPG, the conformations (pearl necklace or core-shell structure) of complexes change differently with increasing surfactant concentration. CSAD molecules form analogous micelle structures through the association within and among molecules in the solution. After the addition of DGP, DGP is adsorbed on the CSAD molecules through a hydrophobic interaction and promotes the association of CSADs, resulting in the decrease in the hydrodynamic diameter of the molecules. With the increase in DGP concentration, more DGP molecules attend the formation of polymer–surfactant complexes, thus explaining the increase in hydrodynamic diameter. When the DGP concentration exceeds CMC, the hydrophilic groups of DGP replace the hydrophilic chain of CSAD to preserve the presence of the hydrophobic micro area. Thus, a part of the polymer–surfactant complexes decomposes and forms pearl necklace structure complexes decorated by small DGP micelles. The amount of pearl necklace structure complexes increases before the DGP concentration surpasses C_2. When the DGP concentration exceeds C_2, a part of pearl necklace structure complexes interact to form core–shell structure complexes with an extremely large hydrodynamic diameter.

In Fig. 10b, CSAD molecules are easier to stretch at the gas–liquid interface because of the shielding effect of NaCl, thus decreasing surface tension significantly. At the same time, the reinforcing effect of NaCl renders the analogous micellar structures formed by CSAD molecules is denser. DGP molecules experience difficultly entering the micellar structures formed by CSAD. Upon entry, they form pearl necklace structure complexes with CSAD directly, thus decomposing the analogous micellar structure. Without polymer–surfactant complexes formed during intermediate processing, DGP reaches CMC early, and abundant pearl necklace structure complexes are formed. CSAD stretches more because of the shielding effect of salt, and DGP molecules easily form micellar structures on CSAD because of the reinforcement effect. Therefore, the addition of NaCl is conducive to the formation of pearl necklace structure complexes. When the DGP concentration reaches C_2, numerous pearl necklace structure complexes interact and develop core-shell structure complexes, and the shielding effect of NaCl facilitates the easy formation of large core-shell structure complexes.

Fig. 10c shows the possible CSAD–DGP interaction at the oil–water interface. Without DGP, CSAD mainly stabilizes the emulsion by coiling onto the oil drop surfaces. Upon the start of DGP addition, DGP molecules make the long chain of CSAD stretch into the continuous water phase, thereby hindering the approach of oil drops and increasing the apparent viscosity of the solution. When C_{DGP} > CAC, more DGP molecules are adsorbed on oil drop surfaces, thereby stabilizing the emulsion and rapidly decreasing oil drop size. DGP molecules connect oil drops by forming micellar structures between CSAD molecular chains. This connection is enhanced as DGP concentration increases, so the *m* of the system decreases. When $C_{DGP} > C_2$, DGP molecules begin to form more independent small DGP micellar structures in the continuous water

phase. Consequently, each small micellar structure only possesses one or two cholesterol groups, thus destroying the network structure and weakening the connection between oil drops. With excessive DGP concentration, DGP molecules occupy most parts of the oil drop surface, and CSAD molecules are crowded out from the oil–water interface. Without the steric hindrance of CSAD, oil drops easily aggregate, and the emulsion becomes unstable.

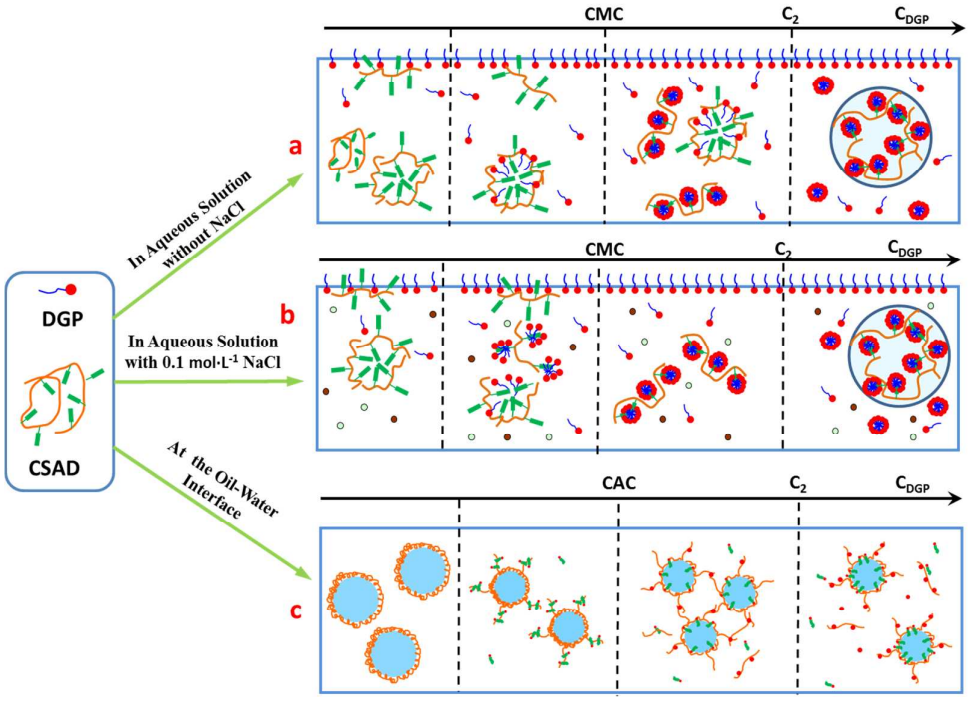

Fig. 10. Schematic of CSAD–DGP interaction in aqueous solutions and at the oil–water interface

4. Conclusions

This study investigated CSAD–DGP interaction in aqueous solution and at the oil–water interface. According to the results of surface tension test and fluorescent spectrometry, DGP and CSAD molecules present competitive adsorption behaviour at the water–gas interface. NaCl can intensify the competitive adsorption behaviour at the water–gas interface. The EPR results indicate that the cholesterol groups of CSAD participate in micellar structure formation. The steric effect of cholesterol groups reduces the microviscosity of micellar structures, and high-concentration NaCl can weaken the polarity of micellar structures and increase their microviscosity. Furthermore, abnormal phenomena of surface tension, fluorescent spectrum, and EPR spectrum were observed under high DGP concentration possibly because high-concentration NaCl facilitates DGP precipitation. However, high-concentration NaCl negatively affects emulsion stability because of the shielding effect of NaCl. Demulsification occurs rapidly. For the emulsion system, the CSAD–DGP interaction could develop a network structure at the oil–water interface, which in turn could enhance the non-Newtonian emulsion properties. However, emulsion retains a low apparent viscosity because of the small oil drop size. When $C_{DGP} > C_2$, excessive DGP micellar structures destroy this network structure. As the DGP concentration increases, DGP replaces CSAD gradually, and almost all CSAD molecules are desorbed from the oil–water interface, resulting in poor stability of the emulsion.

Acknowledgments

We gratefully acknowledge the financial support from the National Natural Science Foundation of China (21366010 and 21566009), the Natural Science Foundation of Hainan Province (213010, 20162013 and 20162016) and Key Projects in the Hainan provincial Science & Technology Program (ZDXM2014037).

References

1. J. Desbrieres, *Cellulose Chemistry & Technology*, 2010, **44**, 395-406.
2. J. Bhattacharjee, G. Verma, V. K. Aswal, V. Patravale and P. A. Hassan, *Rsc Advances*, 2013, **3**, 23080-23089.
3. J. Dey, N. Sultana, S. Kumar, V. K. Aswal, S. Choudhury and K. Ismail, *Rsc Advances*, 2015, **5**.
4. E. Guzmán, S. Llamas, A. Maestro, L. Fernández-Peña, A. Akanno, R. Miller, F. Ortega and R. G. Rubio,

Advances in Colloid & Interface Science, 2015.
5. B. Lindman, A. Khan, E. Marques, M. D. G. Miguel, L. Piculell and K. Thalberg, *Pure & Applied Chemistry*, 1993, **65**, 953-958.
6. K. Shirahama, M. Tohdo and M. Murahashi, *Journal of Colloid & Interface Science*, 1982, **86**, 282-283.
7. R. Nagarajan, *Colloids & Surfaces*, 1985, **13**, 1-17.
8. K. Chari, *Journal of Colloid & Interface Science*, 1992, **151**, 294-296.
9. J. Huang, J. Li, Y. Feng, K. Li, H. Yan, P. Gao, T. Xiao and C. Wang, *Colloids & Surfaces A Physicochemical & Engineering Aspects*, 2015, **479**, 11-17.
10. M. T. L. Casford, P. B. Davies and D. J. Neivandt, *Langmuir*, 2003, **19**, 7386-7391.
11. L. B. Petrovic, V. J. Sovilj, J. M. Katona and J. L. Milanovic, *Journal of Colloid & Interface Science*, 2010, **342**, 333-339.
12. J. C. Marshall, T. Cosgrove, K. Jack and A. Howe, *Langmuir*, 2002, **18**, 9668-9675.
13. E. Akiyama, A. Kashimoto, H. Hotta and T. Kitsuki, *Journal of Colloid & Interface Science*, 2006, **300**, 141-148.
14. J. Philip, G. G. Prakash, T. Jaykumar, P. Kalyanasundaram, O. Mondain-Monval and B. Raj, *Langmuir*, 2002, **18**, 4625-4631.
15. J. S. Nambam and J. Philip, *Journal of Colloid & Interface Science*, 2012, **366**, 88–95.
16. S. N. Pawar and K. J. Edgar, *Biomaterials*, 2012, **33**, 3279-3305.
17. R. Liu, W. Pu, L. Wang, Q. Chen, Z. Li, Y. Li and B. Li, *Rsc Advances*, 2015, **5**.
18. C. Wang, Y. Feng, Q. Lin, H. Yan, X. Chen, J. Huang and J. Li, *Chinese Journal of Pesticide Science*, 2015, **17**, 208-214.
19. L. Yang, B. Zhang, L. Wen, Q. Liang and L. M. Zhang, *Carbohydrate Polymers*, 2007, **68**, 218–225.
20. F. S. Lima, I. M. Cuccovia, B. Richard, F. E. Antunes, L. Bj?Rn, M. G. Miguel, H. Dominik and C. Hernan, *Langmuir*, 2015, **31**, 2609-2614.
21. A. C. F. Ribeiro, I. Fabela, A. J. F. N. Sobral, L. M. P. Verissimo, M. C. F. Barros, M. M. Rodrigo and M. A. Esteso, *Journal of Chemical Thermodynamics*, 2014, **74**, 263-268.
22. A. C. F. Ribeiro, A. J. F. N. Sobral, S. M. N. Simões, M. C. F. Barros, V. M. M. Lobo, A. M. T. D. P. V. Cabral, F. J. B. Veiga, C. I. A. V. Santos and M. A. Esteso, *Food Chemistry*, 2011, **125**, 1213–1218.
23. DONG, L. X. Shu and Y. Gui, *Acta Chimica Sinica*, 2004, **62**, 674-679.
24. M. Hai, *Acta Physico-chimica Sinica*, 2001, **17**, 338-342.
25. J. Oakes, *J.chem.soc.faraday Trans*, 1972, **68**, 1464-1471.
26. E. Szajdzinska-Pietek, R. Maldonado, L. Kevan and R. R. M. Jones, *Journal of the American Chemical Society*, 2002, **107**, 6467-6470.
27. N. Jiang, P. Li, Y. Wang, J. Wang, H. Yan and R. K. Thomas, *Journal of Colloid & Interface Science*, 2005, **286**, 755-760.
28. Z. Hou, Z. Li and H. Wang, *Colloids & Surfaces A Physicochemical & Engineering Aspects*, 2000, **166**, 243-249.
29. L. Huang, M. Petermann and C. Doetsch, *Energy*, 2009, **34**, 1145-1155.

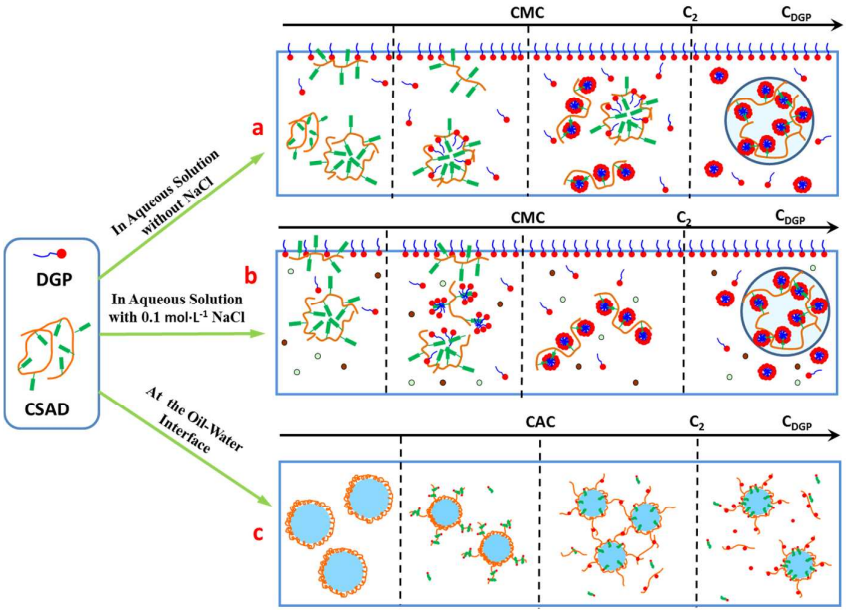

For CSAD/DGP solution systems, the conformations of complexes change differently with the increase in DGP concentration. NaCl can intensify the competitive adsorption behaviors between CSAD and DGP at the water–gas interface. Owing to the reinforcement effect of NaCl, CASD and DGP directly form “pearl necklace” surfactant–polymer complexes. For the emulsion system, CSAD–DGP interaction can develop a network structure on the oil–water interface, which in turn can enhance the non-Newtonian emulsion properties.